

Optimizing the performance of nickel-like collisionally pumped x-ray lasers

G. J. Pert

Department of Physics, University of York, Heslington, York YO10 5DD, United Kingdom

(Received 20 October 2005; published 14 March 2006)

The development of soft x-ray lasers collisionally pumped by a relatively long prepulse and short main pulse has markedly improved the effectiveness of these devices. As a result it is possible to envisage their use in a well equipped university laboratory. In this note we break down the various elements of the interaction and pumping into their simple components in order to see how relatively simple analytic concepts can be used to identify the best mode of operation. However detailed simulation is still required to identify the actual experimental operating conditions. The scaling results are compared with simulation, confirming the value of this analysis.

DOI: [10.1103/PhysRevA.73.033809](https://doi.org/10.1103/PhysRevA.73.033809)

PACS number(s): 42.55.Vc, 32.30.Rj, 42.60.By, 52.50.Jm

I. INTRODUCTION

Since collisionally pumped x-ray lasers were first demonstrated in 1984 [1] there has been a continual process of development whose goal has been to make devices which are compact and easy to use by a nonspecialist community. The first step in this progression was the use of slab rather than foil targets [2], which allowed a significant reduction in the pump energy and easier target handling. A further reduction in input energy resulted from the introduction of multiple-pulse pumping around 1994 [3,4], whereby much of the wasted energy in the long single pulses needed to establish a low density gradient, could be avoided by allowing the plasma to expand freely between the pulses. This technique also helped to overcome a second problem. In order to achieve a high pumping rate, the electron temperature must be high. Since excitation is rapid, so also is ionization and the system is operated out of ionization equilibrium [5]. The next major step forward was the introduction of a short (CPA) pulse to heat the plasma, thereby separating the plasma production phase from the heating needed for inversion [6]. Since the gain was relatively short lived, travelling wave pumping was needed to match the transit of the gain with laser pulse. This approach was further improved by introducing relatively long delays between the prepulse and main pulse in systems of lower atomic number [7,8]. The final major advance has been the introduction of grazing incidence pumping whereby the main heating beam is brought in at near grazing incidence to the target surface to localize the energy deposition to the region where gain will be generated. Using this technique gains have been observed at wavelengths as low as 100 Å with only about 1 J of pump energy [9–11].

The earliest experiments were carried out with neon-like ions, typically selenium, ytterbium and most popularly germanium. These yielded laser action at around 200 Å. Early experiments with the Ne-like ions showed unexpected behavior in that lasing was observed on the $J=2-1$ lines rather than the predicted $J=0-1$ transitions—the latter having a strong direct monopole excitation from the ground state to the upper laser state. This behavior was ascribed to refraction of the x-ray laser beam in the plasma plume, a result demonstrated by the use of curved targets to compensate the beam [12].

Subsequently this effect was avoided by multiple pulse pumping which allowed the plasma to develop a gentler density profile [3,4].

It was early realized that nickel-like systems were intrinsically more efficient in terms of their quantum efficiency and atomic structure, and laser action in these ions was soon found [13]. However gains were low and energy requirements high. The difficulties in generating Ni-like ion laser action were subsequently realized to be due to rapid over-ionization and to refraction and readily overcome by introducing the double pulse approach [14]. The advantages of Ni-like ions over Ne-like could now be realized.

A major problem for the exploitation of these lasers has been their lack of user friendliness. This has stemmed from the large pump lasers that have been needed in the past. This has had three major handicaps for potential applications, particularly those from a different community, namely cost, size, and repetition rate. In addition the reproducibility of the device has been relatively poor, again mainly stemming from the pump. The introduction of the various techniques discussed above changes this picture. Relatively small, university scale, lasers can be used to pump x-ray lasers in Ni-like ions at above 100 Å [15] wavelengths with reasonable efficiency, the laser operating in a saturated regime. Such devices are competitive, contrasting with proposed FELs in terms of size, availability and convenience, and with harmonic generation for power and temporal coherence.

However to date there are only a few demonstration experiments. The full potential of the devices will only be realized once the designs are optimized for power and other properties. In this paper we examine in some detail the physics of the various processes underlying the laser action. Our approach will be to look at the behavior of the different processes that make up the overall laser to identify useful scalings. The aim is not to replace detailed simulation, but to provide a physical understanding for the complex series of processes that lead to laser action and to act as a guide to the strategies that could be used to improve performance. To that end we examine the conditions under which gain is achieved, and how the prepulse and main pulse can be designed to produce these.

An outline sketch of a typical experiment is shown in Fig. 1. The prepulse beam is incident normally on the surface of

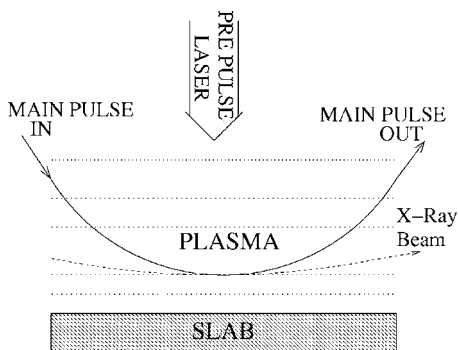


FIG. 1. Schematic diagram showing the arrangement of a typical grazing incidence pumped x-ray laser experiment.

a plane slab target of appropriate material. After a suitable delay the main pulse is incident on the developed plasma at the designated angle. The x-ray beam is formed by spontaneous amplified emission (ASE) in the usual way, following a curved path due to the refraction in the nonuniform plasma. Since the main pulse is short (CPA), travelling wave pumping is required. If the grazing incidence angle is sufficiently small this will occur naturally, but at larger angles may have to be imposed. Even if the pumping lasers are uniform along the plasma length, the plasma will, in practice, have variation in both the normal and transverse directions. However, for this analysis we will assume that the beams are sufficiently wide that the plasma is essentially one dimensional.

We can identify a set of key criteria which must be established:

- (1) The plasma must have the correct ionization. For Ni-like lasers this will be either copper-like or nickel-like.
- (2) The density profile of the plasma must be sufficiently shallow to allow x-rays to traverse the full length.
- (3) The absorption coefficient of the plasma must allow the radiation from the main pulse to be strongly absorbed in the region in which gain is to be generated.
- (4) At the conclusion of the main pulse, plasma must be near the optimal conditions of density, temperature, and ionization.

The prepulse controls plasma formation and thus the density distribution and ionization. The delay between the prepulse and main pulse determines the final density distribution and the ionization at the onset of the main pulse. The main pulse controls the final heating and ionization, and consequently the population inversion.

II. IONIZATION

The laser cannot operate near thermal equilibrium, where in the steady state, ionization and three-body recombination are in balance. Consequently the state must be quasicoronal, with the result that the degree of ionization depends strongly on temperature, but only weakly on density. Figure 2 illustrates this for silver and for samarium in a steady state condition. There is therefore a minimum electron temperature required for the plasma to achieve the required level of ionization. Figure 3 shows the electron temperature to reach the Cu-, Ni-, and Co-like ion stages as a function of the atomic

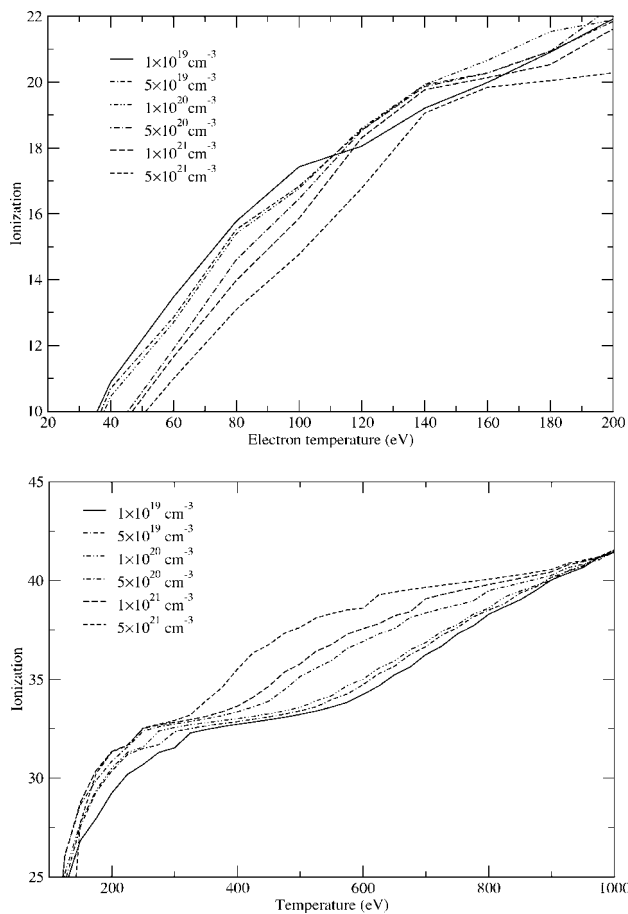


FIG. 2. Steady state ionization of silver(a) and samarium(b) as functions of electron temperature and density.

number for a range of elements at an electron density $5 \times 10^{20} \text{ cm}^{-3}$, using the screened hydrogenic model for the lowest four excited levels. In practice the minimum temperature is that required to have an ionization halfway between the copper-like and nickel-like.

As ionization is relatively slow, we require the plasma to develop its ionization to nearly the required stage during the

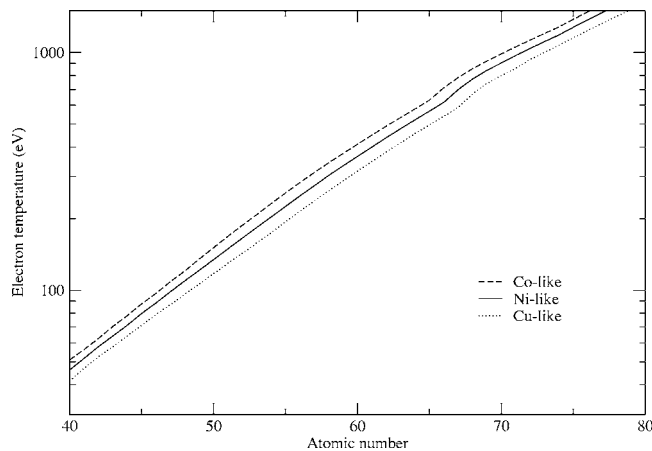


FIG. 3. Electron temperature required to reach various stages of ionization in steady state at electron density $5 \times 10^{20} \text{ cm}^{-3}$.

prepulse phase, provided recombination during any free expansion can be kept small.

This provides two criteria for the specification of the prepulse.

(i) The electron temperature generated during the prepulse must be sufficient to give steady-state ionization at about the nickel-like stage, i.e., the electron temperature must be approximately that given by Fig. 3.

(ii) The time taken to reach steady ionization is given approximately by McWhirter's condition [16],

$$\text{Ionization time} \approx 10^{12}/n_e(\text{cm}^{-3})\text{s}.$$

Thus, for example, if we take $n_e \approx 10^{21} \text{ cm}^{-3}$, then the ionization time is $\sim 10^{-9} \text{ s}$. In fact McWhirter's criterion overestimates the time taken for these cases by up to a factor of 10.

The duration and energy of the prepulse must be sufficient to ensure ionization is nearly complete to steady state. If

these values cannot be consistently achieved it may be necessary to use more energy and overheat the plasma.

III. OPTIMUM PUMPING DENSITY

In a collisionally pumped laser, the population inversion is established between two levels as a consequence of a strong excitation on a radiatively forbidden transition from the ground state to an upper level, which has a strong radiative transition to a second lower level. In this simple three level configuration we may establish a steady state configuration for gain in terms of the rates between the levels. Thus if the levels are numbered 0 (ground), 1 (lower), and 2 (upper), and the radiative and collisional rates are, respectively, A_{ij} and $X_{ij}n_e$ for transitions from level i to j ($A_{20} \approx 0$), we can obtain direct expressions for the populations of the excited states in terms of the population of the ground state n_0 ,

$$\begin{aligned} n_1 &= \frac{(A_{21} + X_{21}n_e)X_{02}n_e + (A_{21} + X_{21}n_e + X_{20}n_e)X_{01}n_e}{(A_{10} + X_{10}n_e + X_{12}n_e)(A_{21} + X_{21}n_e + X_{20}n_e) - (A_{21} + X_{21}n_e)X_{12}n_e} n_0, \\ n_2 &= \frac{(A_{10} + X_{10}n_e + X_{12}n_e)X_{02}n_e + X_{12}n_eX_{01}n_e}{(A_{10} + X_{10}n_e + X_{12}n_e)(A_{21} + X_{21}n_e + X_{20}n_e) - (A_{21} + X_{21}n_e)X_{12}n_e} n_0. \end{aligned} \quad (1)$$

Using the equation of detailed balance [$X_{ij} = X_{ji} \cdot \frac{g_j}{g_i} \exp(-\frac{E_{ji}}{kT})$; $j > i$], it is easy to show that as

$$\begin{aligned} n_e \rightarrow 0, \quad n_1 &\rightarrow \frac{(X_{01} + X_{02})n_e}{A_{10}}, \quad \text{and } n_2 \rightarrow \frac{X_{02}n_e}{A_{21}}, \\ n_e \rightarrow \infty, \quad n_1 &\rightarrow \frac{g_1}{g_0} \exp\left(-\frac{E_{10}}{kT}\right)n_0, \\ \text{and } n_2 &\rightarrow \frac{g_2}{g_0} \exp\left(-\frac{E_{20}}{kT}\right)n_0, \end{aligned} \quad (2)$$

where g_i and E_{i0} are the statistical weight and energy of the state i , respectively. Hence if

$$X_{02}/(g_2A_{21}) > (X_{01} + X_{02})/(g_1A_{10}) \quad (3)$$

a population inversion is established at low density. Since $E_{20} > E_{10}$, the inversion does not occur at high density. Consequently there must exist an optimum electron density at which the population inversion (or the gain) is maximized.

Although this analysis has used a simple three level model, we may note that it is valid quite generally at low densities, where collisional rates are small. The populations in all levels are then determined by a balance between collisional excitation and radiative deexcitation. Indirect pumping is radiative decay from a collisionally pumped level. All populations are therefore linearly proportional to electron

density and the analysis above is valid with a more general interpretation of the rates X_{ij} . Our conclusion that there exists a density for which the population inversion is maximized is therefore unaltered, although of course the value will differ from that given by the three level picture.

Figure 4 show plots of a simple measure of gain for silver and samarium. This measure is taken to be the fractional population inversion in the Ni-like ion multiplied by electron density namely $[(n_2/g_2 - n_1/g_1)/n_{\text{tot}}] \times (10^{-20}n_e)$ where n_{tot} is the total density of Ni-like and Co-like ions. The existence of the optimum density can be clearly seen at about $2 \times 10^{20} \text{ cm}^{-3}$ for silver and 10^{21} cm^{-3} for samarium. We note however that the maximum is relatively broad, so that the optimum does not need to be too tightly achieved.

The plots in Fig. 4 are in fact misleading in that it would appear that the gain is maximized for quite low temperatures. This results from the use of a steady-state model which includes ionization and recombination to and from the cobalt-like next stage of ionization. At the higher temperatures, as can be seen from Fig. 2 the system is completely over-ionized at temperatures above about 125 eV in silver and about 600 eV in samarium. Above these temperatures the total population of the silver or samarium ion is relatively small and the inversion density correspondingly reduced. In fact this highlights a significant problem, which is more severe for Ni-like ions than Ne, namely over-ionization. These lasers are most efficiently pumped out of ionization equilibrium. The gain therefore has a finite lifetime, which is set by

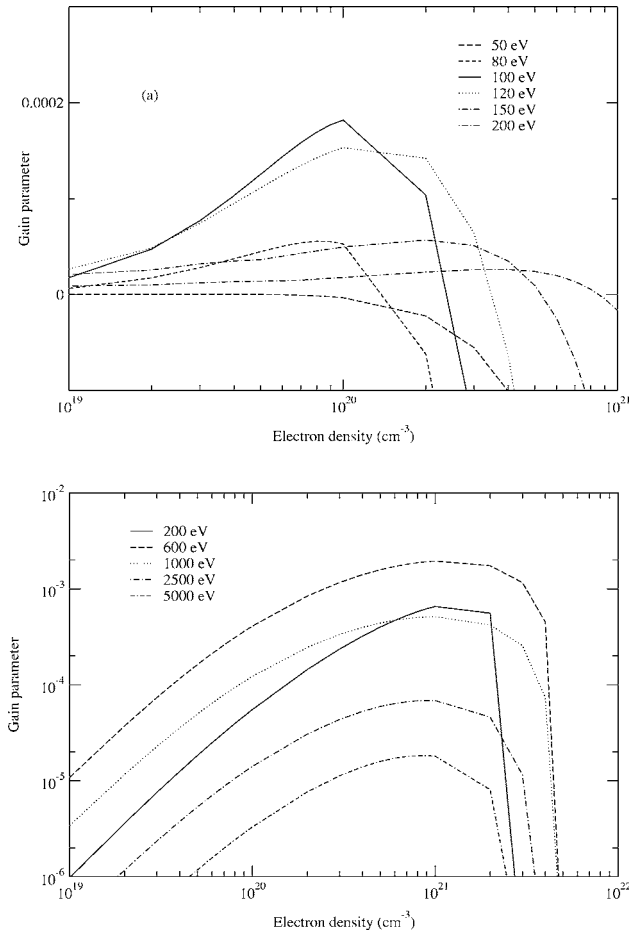


FIG. 4. Plot of the steady state inversion parameter versus electron density at different temperatures for silver (a) and samarium (b).

the ionization time. In fact with modern short pulse pumping methods this problem is avoided, but limited the early experiments with long single pulses [5]. Thus the temperatures for peak gain in Fig. 4 are surprisingly low. In practice because the actual laser system is not in a steady state, as assumed here, it is necessary to increase the pumping rate by increasing the electron temperature generated by the main pulse.

The transient pumping scheme proposed by Afanas'ev and Shlapytsev [17] is the limit of this, in which the excitation pumping rate to the upper laser state is faster than that to the lower, so that a transient inversion is established. Most current designs operate with more balanced pumping over a longer gain lifetime.

The conditions required are typically for silver the electron density about $2 \times 10^{20} \text{ cm}^{-3}$ and temperature about 250 eV: and for samarium density about 10^{21} cm^{-3} and temperature about 1 keV. The difference in these values reflects the change in the ionization state of the Ni-like ion from silver ($Z=19$) to samarium ($Z=34$), and the Z^2 scaling for temperature. The change in density follows from the increased radiative decay probability of the shorter wavelength

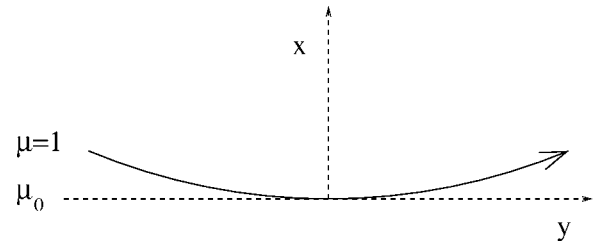


FIG. 5. Ray suffers refraction in the plasma plume.

radiation, which implies that collisional processes must be correspondingly faster.

We remark that the density condition must be satisfied by the prepulse and any subsequent delay, and the temperature by the main pulse.

IV. REFRACTION

As we can see from Fig. 1 refraction plays two important roles in the plasma. First it defines the path of the rays of the main pulse in grazing incidence pumping, and second the paths taken by the x-ray laser beam. It is therefore appropriate to summarize its key behavior in the plasma plume. We consider a one-dimensional plasma with density decreasing normal to the target in the x direction and the beam propagating in the (x,y) plane. The axes are taken through the turning point (perigee) of the ray path $(0,0)$ (Fig. 5). To generalize the picture we define a set of scaling variables $X = \frac{x}{\ell}$ and $Y = \sqrt{\frac{n_0}{(n_c - n_0)}} \frac{y}{\ell}$ where ℓ is the scale length, and n_0 is the density at the perigee and n_c the critical density at the radiation wavelength. Snell's law gives us immediately that

$$\mu \cos \theta = \mu_0 = \cos \theta_0, \quad (4)$$

where θ_0 is the angle of incidence with respect to the surface and μ_0 the refractive index at the perigee.

Assuming that the refraction is solely due to the free electrons with refractive index,

$$\mu = \sqrt{\left(1.0 - \frac{n_e}{n_c}\right)}, \quad (5)$$

the electron density at the turning point is

$$n_0 = n_c \sin^2 \theta_0. \quad (6)$$

For simple plasma distributions, the ray paths are easily evaluated,

$$X = \begin{cases} \frac{1}{4} Y^2, & \text{linear profile,} \\ \ln\left(1 + \frac{1}{4} Y^2\right), & \text{exponential profile.} \end{cases} \quad (7)$$

This result will determine the limiting scale length, which must be established by the prepulse. The value is determined by the condition that x-ray laser rays must remain within the gain zone after refraction. (See Fig. 5.) Thus if the total pumped length of the plasma is L and the thickness of the gain zone d , we can estimate that for a linear profile

$$\ell > \frac{1}{4} \frac{n_0}{n_c - n_0} \frac{L^2}{d}. \quad (8)$$

For grazing incidence pumping, we require that the bulk of the laser energy be deposited near the turning point, rather than absorbed in the extended plasma or reflected out of the system. The absorption coefficient for inverse bremsstrahlung can be written [18] as

$$\kappa = 3.236 \times 10^4 Z \mu^{-1} \lambda^{-2} T^{-3/2} \left(\frac{n_e}{n_c} \right)^2 \ln \Lambda \mu \text{m}^{-1}, \quad (9)$$

with the Coulomb logarithm written as

$$\ln \Lambda = \ln(3.07 \times 10^5 Z^{-1} \lambda T^{3/2}). \quad (10)$$

Hence if the plasma has a uniform temperature $\kappa = \kappa_0 n_e^2$, the absorption length measured from the perigee is

$$\int \kappa ds = \frac{\kappa_0 n_0^2 \ell}{\sin \theta_0} \begin{cases} [2X_2^1 - \frac{4}{3}X_2^3 + \frac{2}{5}X_2^5], & \text{linear profile,} \\ \frac{4}{3}[1 + \frac{1}{2} \exp(-X)] \sqrt{1 - \exp(-X)}, & \text{exponential profile.} \end{cases} \quad (11)$$

Figure 6 shows a plot of this term for different profiles. For effective operation the parameter $\int \kappa ds \approx 1$ or $\kappa \ell \sim \sin \theta_0$. If it is too large the radiation is absorbed in the low density plume, and if too small absorption is weak.

We can also estimate the effect of refraction on the x-ray path length if the gain is uniform. For a linear gradient the path length from the perigee is

$$\int ds = \frac{\mu_0^2 n_c}{n_0} \ell \{ \sqrt{X'(1+X')} + \ln[\sqrt{X'} + \sqrt{1+X'}] \}, \quad (12)$$

where $X' = \frac{n_0 X}{\mu_0^2 n_c}$. In most cases X' is small and $\int ds$ is simply the distance y along the x-ray laser axis.

V. THE PREPULSE PLASMA

We can illustrate the nature of the plasma needed to be generated by the prepulse by considering the two examples of silver and samarium operating with a plasma length of 1 cm. Ni-like silver produces a laser with wavelength 139 Å,

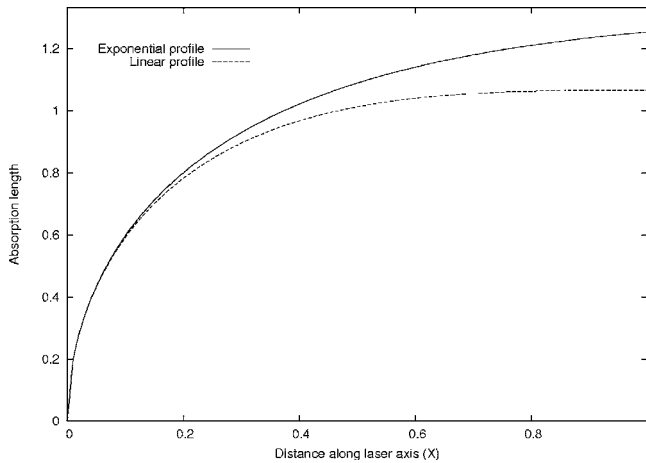


FIG. 6. Normalized absorption length as a function of normalized distance along the plasma axis from the perigee.

the critical density at this wavelength is $5 \times 10^{24} \text{ cm}^{-3}$. Since the optimal density for this laser is $2 \times 10^{20} \text{ cm}^{-3}$, when the gain zone has width 20 μm , the density scale length required is greater than 100 μm . Similarly for samarium the wavelength is 72 Å, the critical density $2 \times 10^{25} \text{ cm}^{-3}$, the optimal density $5 \times 10^{20} \text{ cm}^{-3}$, the gain zone width 10 μm , and the minimum scale length 100 μm .

One point which we may note concerns the scale length. If the spatial scale of the plasma plume is less than the transverse focal spot width the flow will be essentially one dimensional. However once this condition is violated, transverse expansion will cause the density to fall off more rapidly and the prepulse focal spot width essentially provides a limit to the density scale length that can be achieved. The ideal configuration matches the focal spot of the prepulse to the density scale.

VI. SELF-REGULATING MODEL

The structure of the prepulse generated plasma is required to satisfy three conditions, namely density, scale length, and ionization; the latter being essentially a requirement on the temperature. There are two relatively simple models of plasma generation from a slab target by laser heating:

(i) The self-regulating model, which was introduced in the 1960s [19,20], considers plasma heated from the target forming a plume in which inverse bremsstrahlung heating provides the energy source driving the expansion. The plasma self-regulates itself in the sense that the optical depth in the plasma for absorption must be about unity. Referring to Eq. (9) we see that if the plume is too dense, the absorption increases and more energy is absorbed in the plume causing it to expand reducing the density, and *vice versa*. Similar if too hot the absorption is reduced and the plasma cools. The system is therefore stable.

(ii) The deflagration model, introduced slightly later [21,22], allows for the fact that radiation cannot propagate at densities above critical. Hence if the plasma is hot, inverse bremsstrahlung is weak and the radiation is absorbed predominantly near the critical surface by some unspecified

means (nonlinear and/or resonance absorption). This introduces a local heating process closely akin to a classical deflagration in that heat is dispersed from the critical surface, and the width of the active zone determined by thermal conduction. The plasma expands into vacuum in a simple isothermal rarefaction.

It is clear from the above sketches that the self-regulating mechanism applies to low intensity irradiation and the deflagration to high. The limiting condition is that the absorption density is less than or at the critical density. Since we require, at least for the longer wavelengths, a relatively low density, low temperature environment, we would expect that the regime needed for the prepulse is one in which absorption is subcritical (i.e., inverse bremsstrahlung) and thermal conduction relatively weak. In one-dimensional flow these conditions define the time-dependent self-regulating model applicable to low intensity, moderately short pulses. However due to the relatively high state of ionization and long wavelengths used, the atomic density at the critical surface is quite low and the latter will occur quite far into the flow. As a result the flow is not perfectly separated into either the self-regulating or deflagration regimes. It is a relatively simple task to combine the two into a single model. We replace the exit rarefaction from the deflagration by a self-regulating region downstream, using the upstream structure of the deflagration [23] and a truncated form of the steady flow model for self-regulation [24]. However as the resultant flow is not expressible in terms of a similarity analysis, and therefore loses the essential scaling features, it will not be discussed further. However as we shall show self-regulating flow is reasonably accurate for the cases we consider, and will allow us to illustrate the essential physical features of the flow, without giving accurate results.

The early form of the self-regulating model, based around the self-regulating condition, was more formally developed by the author using a self-similar description [25,24]. The characteristic scaling forms follow immediately, with a characteristic self-similar profile scaling for constant power P and pulse length τ as

$$\text{density as } \rho \sim b^{-3/8} P^{1/4} \tau^{-3/8},$$

$$\text{internal energy as } i \sim b^{1/4} P^{1/2} \tau^{1/4},$$

$$\text{distance as } x \sim b^{1/8} P^{1/4} \tau^{9/8},$$

where $b = 5.492 \times 10^{36} (\alpha^{3/2} Z^{9/2} / A^{7/2}) \lambda^2 \ln \Lambda$ and $\alpha = [1 + T_i / (Z T_e)]$, T_i and T_e being the ion and electron temperatures, respectively. Note that these scaling forms immediately lead to the self-regulating condition. The accurate spatial profiles of these quantities are shown in Fig. 7.

The prepulse has two independent control variables: the energy (or power) per unit area and the duration of the pulse. However we have three conditions which we wish to satisfy: the scale length, the ionization, and the density. It is by no means obvious that we can achieve this.

To illustrate this problem we consider silver. Taking a typical experimental value of the intensity namely $1 \times 10^{12} \text{ W cm}^{-2}$ with a prepulse wavelength of $1 \mu\text{m}$. For a gain zone width of $20 \mu\text{m}$ we require a scale length of

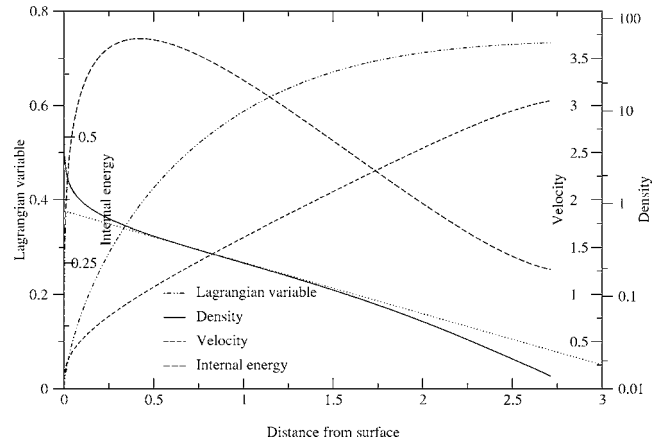


FIG. 7. The scaled distribution of the principal parameters in a self-regulating flow. The dotted line shows the best-fit exponential density profile.

$200 \mu\text{m}$. Hence we find that we require the following pulse lengths are necessary to achieve the required conditions of density, temperature, and scale length:

$$\text{density, } 2 \times 10^{20} \text{ cm}^{-3}, \quad \text{pulse length, } 8000 \text{ ps,}$$

$$\text{temperature, } 100 \text{ eV, } \quad \text{pulse length, } 1 \text{ ps,}$$

$$\text{scale length, } 200 \mu\text{m, } \quad \text{pulse length, } 10 \text{ ps.}$$

Since the scaling is relatively weak, it is clear that we must introduce an additional freedom to the problem. A free expansion following the prepulse allows this situation to be resolved with no further energy input by relaxing the conditions on density and scale length at the end of the prepulse, provided recombination and thermal conduction are weak. We can estimate the values of the input power, pulse length, and delay by the following argument. Since the ionization and necessary temperature must be determined by conditions during heating phase, the product $P^2 \tau$ is determined. But in a one-dimensional expansion the product ρx is invariant, which sets $P^2 \tau^{3/2}$. Hence the pulse duration τ is obtained from $\rho x / T_e$, and thence the remaining parameters can be estimated.

In contrast samarium allows a reasonable choice of values. For an intensity of $1.4 \times 10^{12} \text{ W cm}^{-2}$ and a gain zone width $10 \mu\text{m}$ we obtain

$$\text{density, } 5 \times 10^{20} \text{ cm}^{-3}, \quad \text{pulse length, } 400 \text{ ps,}$$

$$\text{temperature, } 1000 \text{ eV, } \quad \text{pulse length, } 1000 \text{ ps,}$$

$$\text{scale length, } 200 \mu\text{m, } \quad \text{pulse length, } 1000 \text{ ps,}$$

indicating that a good compromise can be found. Thus no free expansion is required for this shorter wavelength system. In fact direct simulation shows this overestimates the pulse length required due to the failure of the self-regulating model noted earlier. However the model still appears to give a reasonable scaling, but is incorrect quantitatively.

From these results we may conclude that elements of atomic number less than about 55 require some delay be-

tween the prepulse and the main pulse and that the delay increases as the atomic number decreases, as demonstrated experimentally [15]. That from 55 to about 65 no delay is appropriate, and that for elements with $Z > 65$ ideally one would wish to use a shorter wavelength pump.

VII. MAIN-PULSE PUMPING

The main pulse power and duration are relatively easily established. We require the pulse to be efficiently absorbed at the designated density and temperature to achieve efficient pumping. The density is identified by the optimal condition discussed earlier and determines the grazing angle of incidence. The temperature is determined by the need for efficient collisional excitation, but is limited by two considerations:

(1) The optical depth must not become too small to prevent further absorption. From Eq. (9) we see that the absorption coefficient decreases as $T_e^{3/2}$. Thus as the plasma heats the absorption decreases. Since the optical depth is given (11) there is clearly a limiting value to the electron temperature, which can be attained, and therefore to the energy in the pulse. The limiting temperature is

$$T_e \approx \left(\frac{\sin \theta_0}{\kappa' n_0^2 \ell} \right)^{2/3}, \quad (13)$$

where the absorption coefficient has been written $\kappa = \kappa' n_0^2 / T_e^{3/2}$ in terms of the values at the perigee. The energy E absorbed determines the temperature through

$$E \approx \frac{3}{2} n_0 k T_e \left(1 + \frac{T_i}{Z T_e} \right). \quad (14)$$

We need to ensure that the limiting temperature is sufficient to give strong collisional pumping.

Following the self-regulating phase, the optical depth for normal incidence is about 1. The increase in temperature can therefore be accommodated by the $\sin \theta_0$ term in Eq. (11). However further free expansion will decrease n_e and T_e in the ratio $T_e \sim n_e^{2/3}$ and cause a consequent decrease in the absorption coefficient. This may limit the amount of free expansion allowed.

(2) As noted earlier the plasma is not in ionization equilibrium. During and after the heating pulse the plasma will continue to ionize to higher stages. While initially this may be advantageous as the prepulse plasma may be underionized, especially if a free expansion phase has been required. However once in Ni-like stage, further ionization is deleterious. Since this rate is temperature dependent, this will limit the possible temperature if the ionization lifetime becomes less than the gain risetime. Fortunately this is not usually a problem.

The duration of the main heating pulse is limited by two factors. First the density profile must not be significantly changed and second the increased ionization rate due to the high temperature leading to significant ionization into the Co-like and higher stages. In general the pulse length must be less than either of these characteristic times. Typically this limits us to a maximum of about 10 ps operating in this

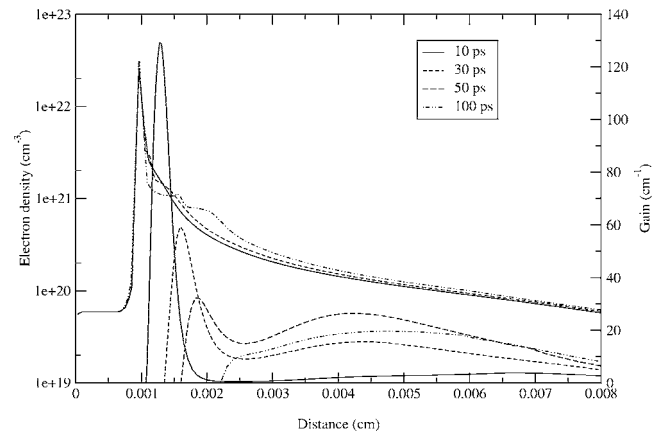


FIG. 8. Electron density and gain profiles as a function of time after the onset of the main pulse for normal incidence pumping for the silver test case.

mode. This condition can be relaxed by operating at lower temperature and lower gain as in the double pulse mode, where pulse lengths are of the order of 100 ps.

We will now examine how these ideas may be used to identify situations in which gain is efficiently generated in the two examples of silver, lasing at 139 Å, and samarium, 72 Å. In each case we will consider an experimental set of pumping conditions based on the most effective systems used to date and using numerical simulation see how well they match to our concepts. The numerical modelling will be carried out using the 1½d code EHYBRID [26,5] developed by the author. Since the cases chosen for study are essentially one dimensional, the simple treatment of transverse expansion in the code leads to small error. This would not be the case if either the prepulse or main pulse had a narrow focal width.

VIII. SILVER

For silver we have identified the optimum density for pumping to be $\sim 2 \times 10^{20} \text{ cm}^{-3}$, and the temperature at the conclusion of the main pulse and any additional ionization required $\sim 200 \text{ eV}$ (Fig. 8). As we noted earlier these conditions cannot be achieved by a prepulse generated by a practical laser alone. Typical prepulse pump conditions used were [8]: 1.06 μm wavelength, 600 ps duration, focal spot 150 μm , and energy 1.5 J/cm. The plasma generated by this prepulse is shown in Fig. 9. It can be seen that the peak temperature achieved is about 80 eV and the peak ionization about 17.5. These values are slightly less than the predicted best values. However note the behavior after the termination of the heating pulse. The electron temperature declines as the plasma cools by expansion. The peak ionization is nearly constant as it moves downstream into lower density. Referring back to Fig. 8 we see that at the onset of the main pulse the optimal density $2 \times 10^{20} \text{ cm}^{-3}$ occurs at about 350 μm where the ionization is slightly below the peak at about 17. This ionization deficit is made up following the final heating by the main pulse.

Normal incidence pumping: The main pulse has charac-

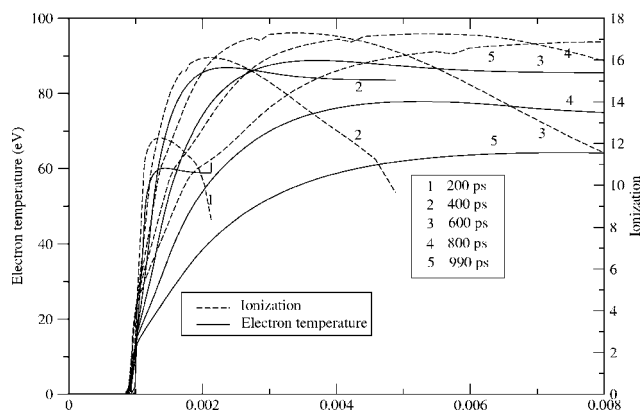


FIG. 9. The development of ionization and electron temperature in the prepulse plasma in silver as a function of time from the onset of the prepulse for the silver test case.

teristics: $1.06 \mu\text{m}$ wavelength, 1 ps duration, focal spot $80 \mu\text{m}$, and energy 2 J/cm . The development of the gain and electron density are shown in Fig. 8. It can be seen that there are two regions of strong gain. The inner with peak gain $\sim 120 \text{ cm}^{-1}$ at density 10^{21} cm^{-3} is associated with heating near the critical density by the pulse. The high density leads to rapid heating, ionization, and subsequent gain. The gain is however relatively short lived as the ionization continues beyond the nickel-like stage. Furthermore the density gradient at this point is too large to allow a large x-ray laser pulse to develop.

The principal region of gain is developed farther out with values $\sim 20 \text{ cm}^{-1}$ at density $1.5 \times 10^{20} \text{ cm}^{-3}$ and temperature 180 eV. The density gradient in this region is sufficiently small to allow strong x-ray laser action over the full length of the plasma accessing the peak gain. This gain peak occurs due the improved efficiency of pumping the inversion resulting from the density scaling of gain discussed earlier. It is also established late due to the need for further ionization after the free expansion phase. In the region of the inner gain peak, the higher electron density gives much faster ionization, and higher peak gain as the electron temperatures at the gain peak are approximately equal.

It is clear from this simulation that much of the main-pulse heating occurs in spatial regions where the gain is inaccessible due to refraction, and that the main-pulse energy is consequently not most effectively used.

Grazing incidence pumping: We now examine the effect of pumping the prepulse plasma at a grazing incidence angle of 26.5° corresponding to density $2 \times 10^{20} \text{ cm}^{-3}$ and reducing the main pulse to 0.5 J/cm . Figure 10 shows the density and gain profiles generated. It can be clearly seen that the gain is strongly developed at the designated heating density. The gain at high density does not occur. The double peaked structure is a consequence of over-ionization in the region of the minimum consequent on the strong local heating. The delay before the development of gain is due to the need for further ionization beyond that achieved by the prepulse plasma. It is clear that significant gain can be generated with reduced energy in the main pulse.

Since the scaling of the prepulse plasma with laser energy is relatively weak, and since the whole of the plasma is

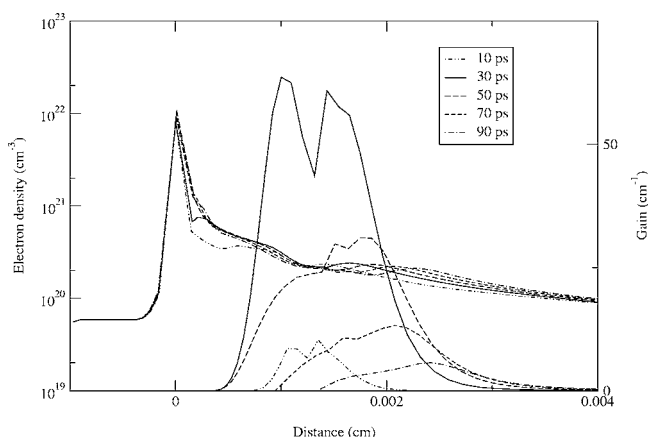


FIG. 10. Electron density and gain profiles in silver as a function of time after the onset of the main pulse for grazing incidence pumping with reduced main-pulse energy only.

heated by the prepulse, it becomes a relevant question to ask whether it is more efficient to relax the ionization condition, i.e., temperature, on the prepulse plasma and allow additional localized heating from the main pulse to generate the additional ionization needed. Figure 11 shows the situation when the prepulse is reduced to 0.5 J/cm , the main pulse being left unchanged at 0.5 J/cm . It can be seen that strong gain is again generated at about $\sim 2 \times 10^{20} \text{ cm}^{-3}$ as required.

IX. SAMARIUM

Normal incidence pumping: We now turn to the case of samarium. Successful experiments were reported by King *et al.* [27]. The system was optimized for the delay between the prepulse and the main pulse, with the best results obtained when the main pulse was applied just after the peak of the prepulse. The pump conditions were modelled with the following values: prepulse, $1.06 \mu\text{m}$ wavelength, 285 ps duration, focal spot $100 \mu\text{m}$, and energy 12.3 J/cm (9 J/cm delivered up to the main-pulse onset); and main pulse, $1.06 \mu\text{m}$ wavelength, 2 ps duration, focal spot $100 \mu\text{m}$, and energy

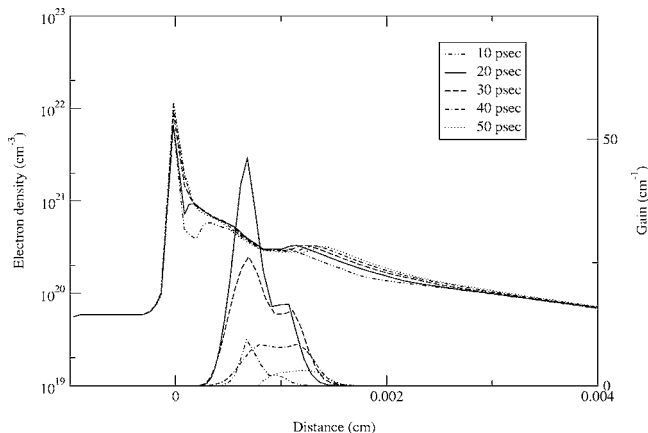


FIG. 11. Electron density and gain profiles in silver as a function of time after the onset of the main pulse for grazing incidence pumping with reduced prepulse and main-pulse energy.

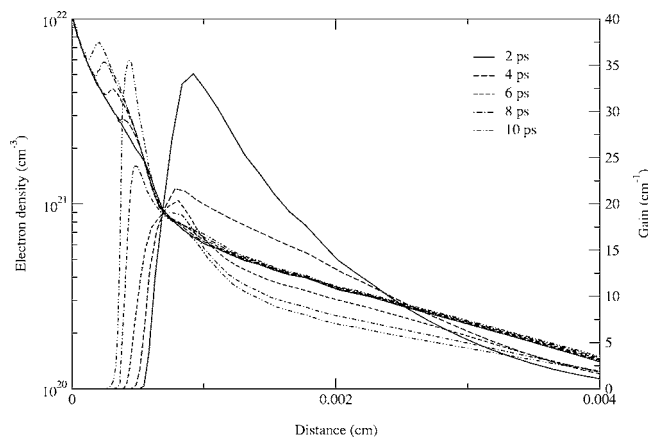


FIG. 12. Electron density and gain profiles from the modelling of the samarium experiments of King *et al.* at normal incidence.

19.8 J/cm, delayed by 290 ps. Figure 12 shows the density and gain profiles for this case. We note that the conditions achieved closely match the optimum values of electron density $\sim 10^{21}$ cm $^{-3}$ and electron temperature ~ 1000 eV. The strongest gain is achieved at near the critical density of the pump laser, $\sim 10^{21}$ cm $^{-3}$, on the edge of the steep density gradient. However ray tracing shows that the spatial extent of gain into the lower density, lower gradient downstream plasma is sufficient to generate a significant output pulse [27].

We note the presence of strong gain occurring at $\sim 2 \times 10^{21}$ cm $^{-3}$, i.e., behind the critical density later. This is due to the following:

(i) Strong thermal conduction from the zone of strong heating into cold plasma due to the strong scaling with temperature ($\sim T_e^{5/2}$).

(ii) Strong ionization at high density.

(iii) Effective gain generation at this density.

It is inaccessible due to the strong refraction in the large density gradient.

Grazing incidence pumping: The presence of the high gain and strong heating in the inaccessible zone behind the absorption shows that pumping should take place at a slightly lower density to maximize the energy usage, i.e., that we should use a grazing incidence pump, despite the fact that it is slightly below the optimal pumping density. Grazing incidence pumping will allow us to generate gain at slightly lower density with less refraction.

As a demonstration case, we consider pumping at a grazing incidence angle of 45° corresponding to density 5×10^{20} cm $^{-3}$, but with the same prepulse energy delivered in a square pulse of 9.0 J/cm to match the delay. The energy is now deposited directly in a region of modest gradient, which allows us to reduce the main pulse to 4.5 J/cm. The results are shown in Fig. 13. The gain is local at $\sim 5 \times 10^{20}$ cm $^{-3}$ with a similar value to that achieved with normal incidence. A similar output to that achieved earlier is expected but with the main pump energy reduced to a third of that needed with normal incidence.

In order to examine whether further improvement could be achieved by modifying the prepulse we introduced the following changes:

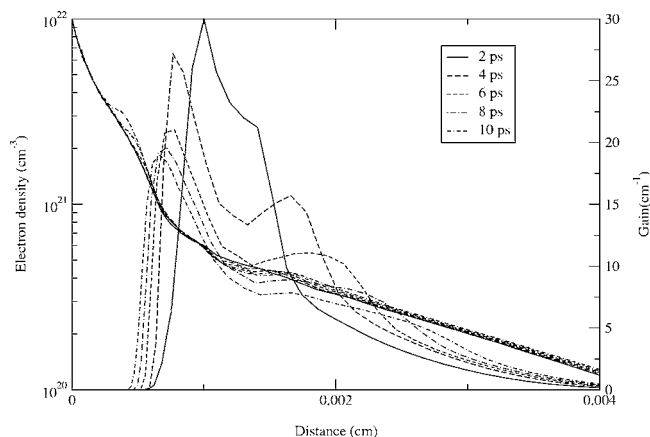


FIG. 13. Electron density and gain profiles from the modelling of the samarium at grazing incidence.

(i) A delay between prepulse and main pulse. This required a larger prepulse energy as cooling and recombination in the expansion phase severely degraded the ionization. This change caused a deterioration in output and was not worth proceeding with.

(ii) Longer prepulse pump to maintain ionization, but the level required is at the same intensity as before so that the prepulse energy is increased. The advantage is a longer plasma body with weaker gradient, which suggests using a slightly decreased grazing angle and operating at a lower density. The result is a longer gain duration which is more widely distributed, but overall the increased output did not justify the additional prepulse energy required.

X. DISCUSSION

We have presented a relatively simple analysis of the development of the grazing incidence pumped x-ray laser by breaking the various aspects of gain generation down into their basic components and examining the conditions necessary to establish their best operation. This has led to a relatively simple set of necessary conditions on the prepulse for optimization, and less stringent requirements on the main pulse. The analysis involves the use of simple plasma generation model, known to be inexact, but gives a useful approximate scaling. Accurate determination of the conditions requires the detailed simulation. To illustrate the limitations on the analysis we may compare the values calculated by the self-regulating model for the simulations in silver and samarium.

In silver we have for a pulse of 150 J cm $^{-2}$ and duration 600 ps, at 1 μ m wavelength, direct simulation gives a peak temperature of 86 eV at density 1.4×10^{20} cm $^{-3}$ with a scale length 16 μ m. The self-regulating model gives characteristic density 3.7×10^{19} cm $^{-3}$, electron temperature 315 eV. and scale length 53 μ m. However if we take into account the energy required for ionization, the unmatched focal spot width and energy reflected, the effective energy reduces to 50 J cm $^{-3}$ and the values become density 3×10^{20} cm $^{-3}$, temperature 174 eV and scale length 40 μ m, in much closer agreement. We may further correct for the actual self-similar

values from Fig. 7 which give a peak temperature of 0.695 at density 0.5 and scale length 0.78 to give 121 eV, $1.5 \times 10^{20} \text{ cm}^{-3}$ and $30 \mu\text{m}$, respectively. The agreement is respectable.

For the samarium simulation we have a pulse of 900 J cm^{-2} and duration 300 ps also at $1 \mu\text{m}$ wavelength. Direct simulation gives a peak temperature of 440 eV at density $2 \times 10^{20} \text{ cm}^{-3}$ with a scale length $20 \mu\text{m}$. The corrected input energy is 420 J cm^{-2} , the self-regulating values after correction are density $2.6 \times 10^{20} \text{ cm}^{-3}$, temperature 506 eV, and scale length $36 \mu\text{m}$: the agreement is again acceptable, provided the necessary corrections are made.

We may note however that in both the above cases, the peak of the gain occurs in Lagrangian cells which lie at higher density in the expansion, but where the ionization and temperature at the end of the prepulse are not too dissimilar from the values noted above.

From this analysis we can identify relatively broad specifications for the conditions under which gain can be optimized. These are based around a set of reasonably simple criteria:

- (i) In short pulse pumping, the plasma density profile is established by the prepulse.
- (ii) The temperature is determined by the main pulse.
- (iii) Ionization depends on the pulse configuration.
- (iv) Longer wavelength elements benefit from delays between the pulses.
- (v) Shorter wavelength elements require the main pulse to start at the conclusion of the prepulse to avoid cooling and recombination.
- (vi) Grazing incidence pumping by localizing the energy

deposition of the main pulse, can be used to reduce the required energy input.

(vii) Significant improvements in the overall efficiency are possible, and make available lasers of much wider accessibility.

As we have seen these systems with pumping on the fundamental lines of Nd-YAG or Ti-sapphire at wavelengths between $0.8\text{--}1 \mu\text{m}$ are limited to atomic numbers ≤ 62 by the need to separate the pumped plasma from the solid/plasma interface. If the latter can be pushed to higher density then it should be possible to generate a reasonably flat zone in which the x-ray laser pulse can propagate. This is easily achieved by decreasing the wavelength of the prepulse by using a harmonic. The main pulse can still be the fundamental introduced normally up to a pumping density of $\sim 10^{21} \text{ cm}^{-3}$, but for convenience grazing incidence pumping at the harmonic may be preferred.

In this analysis we have assumed that the plasma development is one dimensional. In the case of the prepulse, this is probably necessary as the scale length will be limited by the focal spot width once two-dimensional effects become significant. The main pulse however can be made significantly narrower as thermal losses transversely are likely to be small compared to the lateral ones, provided the spot is not too narrow. This will allow a corresponding reduction in the required pumping energy, a technique which has already been used in normal pumped experiments [8].

ACKNOWLEDGMENTS

It is a pleasure to acknowledge the helpful discussions with Professor G. J. Tallents and T. A. Ball on this topic. This work was in its early stages supported by EPSRC and AWE.

-
- [1] D. Matthews *et al.*, Phys. Rev. Lett. **54**, 110 (1985).
 - [2] T. N. Lee, E. McLean, and R. C. Elton, Phys. Rev. Lett. **59**, 1185 (1987).
 - [3] J. Nilsen and J. C. Moreno, Phys. Rev. Lett. **74**, 3376 (1995).
 - [4] H. Daido *et al.*, Opt. Lett. **20**, 61 (1995).
 - [5] P. Holden *et al.*, J. Phys. B **27**, 341 (1994).
 - [6] P. V. Nickles, V. N. Shlyaptsev, M. Kalachnikov, M. Schnurer, I. Will, and W. Sander, Phys. Rev. Lett. **78**, 2748 (1997).
 - [7] J. Dunn, A. L. Osterheld, R. Shepherd, W. E. White, V. N. Shlyaptsev, and R. E. Stewart, Phys. Rev. Lett. **80**, 2825 (1998).
 - [8] J. Dunn, Y. Li, A. L. Osterheld, J. Nilsen, J. R. Hunter, and V. N. Shlyaptsev, Phys. Rev. Lett. **84**, 4834 (2000).
 - [9] R. Keenan *et al.*, Proc. SPIE **5197**, 213 (2003).
 - [10] R. Keenan, J. Dunn, P. K. Patel, D. F. Price, R. F. Smith, and V. N. Shlyaptsev, Phys. Rev. Lett. **94**, 103901 (2005).
 - [11] B. Luther *et al.*, Opt. Lett. **30**, 165 (2005).
 - [12] R. Kodama, D. Neely, Y. Kato, H. Daido, K. Murai, G. Yuan, A. MacPhee, and C. L. S. Lewis, Phys. Rev. Lett. **73**, 3215 (1994).
 - [13] B. MacGowan, S. Maxon, P. L. Hagelstein, C. J. Keane, R. A. London, D. L. Matthews, M. D. Rosen, J. H. Scofield, and D. A. Whelan, Phys. Rev. Lett. **59**, 2157 (1987).
 - [14] J. Zhang *et al.*, Science **276**, 1097 (1997).
 - [15] Y. Wang *et al.*, Phys. Rev. A **72**, 053807 (2005).
 - [16] R. McWhirter, in *Plasma Diagnostic Techniques*, edited by R. Huddleston and S. Leonard (Academic, New York, 1965), Chap. 5, pp. 201–264.
 - [17] I. Afanas'ev and V. Shlyaptsev, Sov. J. Quantum Electron. **19**, 1606 (1989).
 - [18] J. Dawson and C. Oberman, Phys. Fluids **5**, 517 (1962).
 - [19] I. Afanas'ev, V. Krol, O. Krokhin, and I. Nemchinov, J. Appl. Math. Mech. **30**, 1218 (1966).
 - [20] A. Caruso, B. Bertotti, and P. Giupponi, Nuovo Cimento A **45**, 176 (1966).
 - [21] C. Fauquignon and F. Floux, Phys. Fluids **13**, 386 (1970).
 - [22] J. Bobin, Phys. Fluids **14**, 2341 (1971).
 - [23] G. J. Pert, J. Plasma Phys. **29**, 415 (1983).
 - [24] G. J. Pert, J. Plasma Phys. **36**, 415 (1986).
 - [25] G. J. Pert, J. Plasma Phys. **35**, 43 (1986).
 - [26] G. J. Pert, J. Fluid Mech. **141**, 401 (1983).
 - [27] R. King *et al.*, Phys. Rev. A **64**, 053810 1 (2001).